J Sol-Gel Sci Technol (2017) 81:483–492
DOI 10.1007/s10971-016-4212-z

ORIGINAL PAPER: NANO-STRUCTURED MATERIALS (PARTICLES, FIBERS, COLLOIDS, COMPOSITES, ETC.)

Investigation of structural, morphological, optical, and magnetic properties of Sm-doped $LaFeO_3$ nanopowders prepared by sol–gel method

Ekaphan Swatsitang[1,2] · Attaphol Karaphun[1,2] · Sumalin Phokha[3] · Sitchai Hunpratub[3] · Thanin Putjuso[4]

Received: 1 May 2016 / Accepted: 18 September 2016 / Published online: 7 October 2016

Abstract Pure orthorhombic phase of $La_{1-x}Sm_xFeO_3$ ($x = 0$, 0.1, 0.2, and 0.3) nanoparticles can be obtained by sol–gel method after calcination at 800 °C for 3 h in air. X-ray diffraction, scanning electron microscopy, transmission electron microscopy, X-ray photoelectron spectroscopy, Fourier transform infrared spectroscopy, X-ray absorption near edge spectroscopy, ultraviolet-visible spectroscopy, and vibrating sample magnetometry were used to study the crystal structure, morphology, oxidation state, functional group, optical, and magnetic properties of samples. Pure orthorhombic phase of perovskite structure is confirmed by X-ray diffraction results. Decreasing lattice parameters, crystallite sizes, and cell volumes with increasing micro-strains indicate structure distortion due to the substitution of Sm ions with small ionic radius on the La sites in the orthorhombic structure. Scanning electron microscopy and transmission electron microscopy images show a homogeneous distribution of almost spherical nanoparticles with decreasing average particle sizes ranging from 56.48 ± 3.22 to 23.21 ± 4.40 nm for samples of high Sm content. Fourier transform infrared spectroscopy spectra confirm the Fe–O stretching mode in octahedral FeO_6 unit of a perovskite structure. X-ray photoelectron spectroscopy and X-ray absorption near edge spectroscopy results indicate the oxidation states +3 of La and Fe ions. The optical band gaps are found to decrease from 2.218 to 1.880 eV with increasing Sm content. vibrating sample magnetometry results show the antiferromagnetic behavior of undoped sample and ferromagnetic behavior for doped samples, affecting by structure distortion and particle size reduction. Interestingly, the coercive field is significantly enhanced from 95.07 Oe ($x = 0.1$) to 13,062.79 Oe ($x = 0.3$). Curie temperature (T_c) is suggested to be above 400 K.

Graphical Abstract The magnetization curves of $La_{1-x}Sm_xFeO_3$ ($x = 0.0$, 0.1, 0.2, and 0.3) nanoparticles prepared by the sol-gel method with the inset show the comparing coercive forces (Hc) of the present work and the previous works, $La_{0.7}M_{0.3}FeO_3$ (M = Al and Ga). Sm-doped $LaFeO_3$ nanoparticles can exhibit ferromagnetic behavior with the significant enhancement of Hc from 95.07 to 13,062.79 Oe.

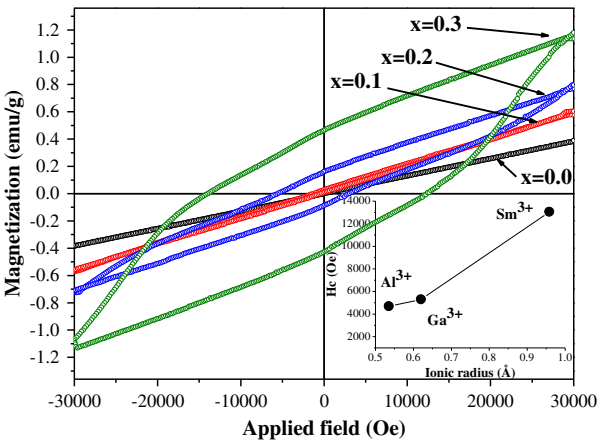

✉ Thanin Putjuso
thanin.put@rmutr.ac.th
putjuso@hotmail.com

1 Integrated Nanotechnology Research Center, Department of Physics, Department of Science, Khon Kaen University, Khon Kaen 40002, Thailand

2 Nanotec-KKU Center of Excellence on Advanced Nanomaterials for Energy Production and Storage, Khon Kaen 40002, Thailand

3 Department of Physics, Department of Science, Udon Thani Rajabhat University, Udon Thani 41000, Thailand

4 Rajamangala University of Technology Rattanakosin Wang Klai Kangwon Campus, Prachuap Khiri Khan 77110, Thailand

Keywords Sm-doped $LaFeO_3$ · Sol–gel method · Optical properties · Magnetic properties

1 Introduction

Pure and doped lanthanide orthorhombic perovskites, such as $LaFeO_3$, $BiFeO_3$, $GdFeO_3$, $NdFeO_3$, $SmFeO_3$, and etc. [1–3] continue to attract significant attention as a promising material for applications in solid oxide fuel cells [4], catalysts [5], chemical sensors [6], thermoelectric [7], and magnetic materials [8–10]. Among these materials, lanthanum orthoferrite ($LaFeO_3$) is the common one that has been widely studied because it can exhibit ferroelectric and ferromagnetic properties [11] similar to those observe in $BiFeO_3$ [12, 13]. However, bulk $LaFeO_3$ is known to be an antiferromagnetic material with a very high Néel temperature (T_N) of 738 K [14] owing to the stability of a magnetic structure of the collinear arrangement of FeO_6 octahedral units in the two interpenetrating pseudo cubic face-centered sublattices [15–19]. Therefore, many researchers attempt to improve its magnetic property by replacement of La and/or Fe sites with various metal ions. For instance, ferromagnetic behavior can be obtained in $La_{1-x}Al_xFeO_3$ [20], $La_{1-x}Ga_xFeO_3$ [21], $LaFe_{1-x}Mg_xO_3$ [2], $La_{1-x}Ca_xFeO_3$ [22], $La_{1-x}Ce_xFeO_3$ [23], $La_{1-x}Cu_xFeO_3$ [24], $La_{1-x}Pb_xFeO_3$ [25], and $LaFe_{1-x}Ti_xO_3$ [26]. These substitutions induced the distortion of the structure and the reduction of particle size, resulting in uncompensated surface spins [25, 27]. Normally, pure and doped $LaFeO_3$ can be prepared by various techniques, such as electrospinning [28], hydrothermal [29], microwave-assisted method [30], sonochemical method [31], modified solution combustion method [32], sol–gel [33–35] and polymerization complex method [20, 21]. From these synthesis methods, sol–gel method is widely employed for the synthesis of nanoparticles because of the simplicity, low cost, homogeneous dispersion of nanoparticles and most of all, products of pure phase can be obtained. Sm of smaller ionic radius (0.958 Å) than that of La (1.27 Å), but with the same oxidation state +3 is another interesting lanthanide metal that expect to replace the La site to effect the structure distorsion and improve the magnetic property of $LaFeO_3$ similar to those observe in our previous works [20, 21].

In this work, $La_{1-x}Sm_xFeO_3$ ($x = 0.0$, 0.1, 0.2, and 0.3) nanoparticles were prepared by sol–gel method. The structural, morphological, optical, and magnetic properties of the obtained products were studied by X-ray diffraction (XRD), scanning electron microscopy (SEM), transmission electron microscopy (TEM), Fourier transform infrared spectrophotometry (FTIR), Ultraviolet-visible spectrophotometry (UV–vis), X-ray photoelectron spectroscopy (XPS), X-ray absorption near edge spectroscopy (XANES) and vibrating sample magnetometry (VSM). Interestingly, very high coercive force (H_c) can be obtained, comparing with those of our previous works [20, 21].

2 Experimental

In the synthesis of $La_{1-x}Sm_xFeO_3$ ($x = 0.0$, 0.1, 0.2, and 0.3) nanoparticles by sol–gel method, the stoichiometric amounts of $Fe(NO_3)_{3.9}H_2O$ (Kento chemical Co., 99.9 %), $LaN_3O_9.6H_2O$, (Fluka, 99.0 %), and $Sm(NO_3)_3{\cdot}6H_2O$ (Aldrich, 99.9 %) by a ratio of 1:1 (Fe:La,Sm) with 40 g of $C_6H_8O_7.H_2O$ (VWR International Ltd., 99.7 %), were firstly dissolved in a mixture of 60 ml deionized water and 120 ml of ethylene glycol under a mechanical stirring at room temperature using a magnetic bar. Secondly, this solution was heated at 80 °C under a constant stirring until a gel was formed and dried. The final products were pre-calcined at 400 °C for 3 h in air and ground to fine powders. These powders were further calcined at 800 °C for 3 h in air to obtain the perovskite phase of $LaFeO_3$.

Phase and structure of the products were investigated by XRD (SHIMADZU, XRD-6100) with CuKα_1 radiation ($\lambda = 1.5405$ Å). The XRD peaks were indexed according to the standard data of $LaFeO_3$ (JCPDS no. 37–1493). Scanning electron microscope (SEM, 1450VP, LEO UK) and TEM (TECNAI G2 20, FEI) were employed to observe the morphology, particle size determination, and the dispersion of particles. The FTIR spectra of all samples were obtained by FTIR (spectrum one FTIR, Perkin Elmer Instrument, USA) in the wavenumber range from 400 to 4000 cm^{-1}, using the KBr pellet technique. UV–vis (Shimadzu UV-3101PC) was employed for the optical properties study of the products in the wavelength from 200 to 800 nm. X-ray photoelectron spectroscopy (XPS, AXIS Ultra DLD, Kratos Analytical Ltd. Manchester UK) was used to investigate the oxidation state of La, Fe and O ions in the structure of $La_{0.7}Sm_{0.3}FeO_3$ nanoparticles. Fe K-edge XANES spectra of standard metals and samples of $x = 0.0$ and 0.3 were obtained in a transmission mode at the BL5.2 of Synchrotron Light Research Institute in Nakhon Ratchasima, Thailand. Room temperature magnetizations of all samples were measured by the vibrating sample magnetometer (VSM, Versa Lab™ free, Quantum Design USA) in the magnetic field range of ±30 kOe. Temperature variation of the magnetization for sample of $x = 0.3$ was performed in the field cooling (FC) and zero field cooling (ZFC) modes from 50–390 K under an external magnetic field (H) of 10 kOe.

3 Results and discussion

XRD patterns of $La_{1-x}Sm_xFeO_3$ ($x = 0.0$, 0.1, 0.2, and 0.3) nanoparticles are shown in Fig. 1. It is obvious that all samples have the perovskite structure of orthorhombic phase as indexed in the standard data of $LaFeO_3$ (JCPDS no. 37–1493). The average crystallite sizes of samples were calculated from the dominant peaks of X-ray line

broadening of the (101), (121), (220), (202), and (123) planes using Scherrer equation,

$$D_{Sch} = (k\lambda)/(\beta cos\,\theta) \quad (1)$$

where D_{Sch} is the average crystallite size, θ is the Bragg angle, λ is the wavelength of the X-ray, β is the full width at half maximum, the constant k is taken as 0.9 [36]. The obtained results as summarized in Table 1 show that the average crystallite sizes decrease with increasing Sm content as shown in the inset of Fig. 1 and found to be 58.45 ± 5.90, 30.22 ± 6.32, 23.25 ± 3.64, and 16.96 ± 4.23 nm for samples of $x = 0.0$, 0.1, 0.2, and 0.3, respectively. The lattice parameters (a, b, and c) and cell volumes of samples were calculated by Rietveld refinement method with the GOF, R_{wp}, and R_p in the range of 1.97–2.87 %, 6.09–8.19 %, and 4.53–6.29 %, respectively. All of these parameters are summarized in Table 1. It can be seen that the calculated lattice parameters are in good agreement with those of the orthorhombic phase of $LaFeO_3$ and found to decrease in samples of high Sm content due to the replacement of a larger ionic radius La^{3+} ion by a smaller ionic radius Sm^{3+} ion. Similarly, the cell volumes are decreased in the same manner as well. In addition, the crystallite size and the microstrain of samples were also calculated for the comparison by using the Williamson-Hall equation [37],

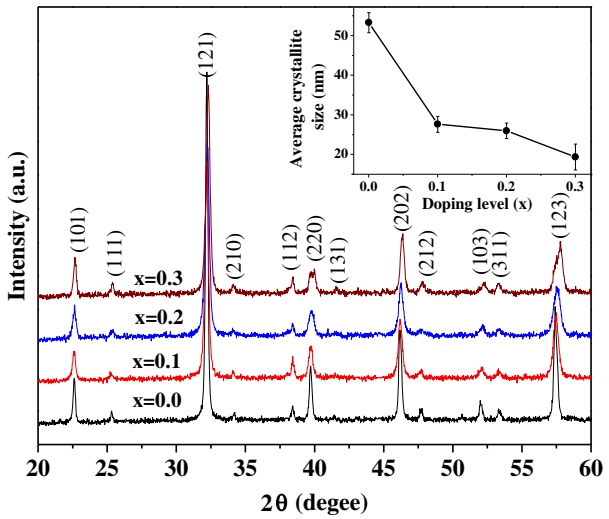

Fig. 1 XRD patterns of $La_{1-x}Sm_xFeO_3$ ($x = 0.0$, 0.1, 0.2, and 0.3) nanoparticles

$$\beta\, cos\theta = (k\lambda)/D_{Sch} + 2\varepsilon \sin\theta \quad (2)$$

where D_{WH} is the average crystallite size, θ is the Bragg angle, λ is the X-ray wavelength, $k = 0.9$, β is the full width at half maximum of XRD peaks and ε is the microstrain of the lattice. The plots of βcosθ as a function of sinθ are shown in Fig. 2. D_{WH} and ε of samples are determined from the linear extrapolation and slope of these plots, respectively. All of these values are summarized in Table 1 and it is found that D_{WH} decrease from 60.31 to 28.95 with increasing Sm content, while those of ε increase from 0.0005 to 0.0033 due to the shrinkage of the lattice parameters. These results are in good agreement with the decrease of cell volumes of the $La_{1-x}Sm_xFeO_3$ ($x = 0.0$, 0.1, 0.2, and 0.3) crystals.

TEM images with selected area electron diffraction (SAED) patterns of $La_{1-x}Sm_xFeO_3$ ($x = 0.0$, 0.1, 0.2 and 0.3) nanoparticles are shown in Fig. 3. It can be seen that all samples compose of almost spherical nanoparticles with the estimated average sizes (D_{TEM}) using Image J program decrease from 56.48 ± 3.22 to 23.21 ± 4.40 nm due to the increase of Sm ion in the structure, as summarized in Table 2. SAED patterns of these samples (insets of Fig. 3) show ring patterns, indicating a polycrystalline of doped samples and they can be indexed to a certain crystalline

Table 1 Lattice parameters (a, b, and c), cell volume (V), R_p (profile), R_{wp} (weighted profile), GOF (goodness of fit), crystallite sizes by Scherrer (D_{Sch}), and Williamson-Hall (D_{WH}) with microstrain (ε) of $La_{1-x}Sm_xFeO_3$ ($x = 0.0$, 0.1, 0.2, and 0.3) nanoparticles

Parameters	$La_{1-x}Sm_xFeO_3$			
	$x = 0.0$	$x = 0.1$	$x = 0.2$	$x = 0.3$
Lattice parameters (Å)				
a	5.563	5.571	5.571	5.577
b	7.852	7.840	7.827	7.810
c	5.553	5.543	5.530	5.510
V(/10^6 pm^3)	242.60	242.11	241.15	240.06
R_p (profile) %	6.29	5.62	4.79	4.53
R_{wp} (weighted profile) %	8.19	7.73	6.43	6.09
GOF (goodness of fit)	2.87	2.66	1.97	2.02
Crystallite size (nm)				
D_{Sch}	53.03 ± 2.53	27.64 ± 2.03	25.99 ± 1.96	19.39 ± 2.28
D_{WH}	60.31	34.36	32.16	28.95
Microstrain (ε)	0.0005	0.0014	0.0015	0.0033

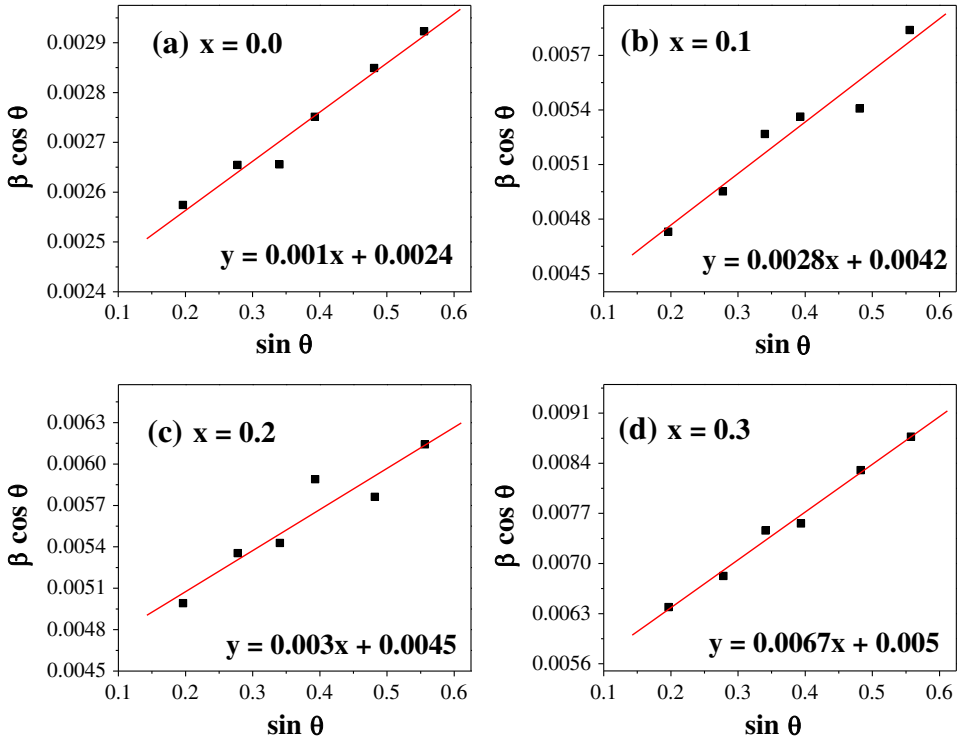

Fig. 2 Williamson-Hall plots of $La_{1-x}Sm_xFeO_3$ nanoparticles. **a** $x = 0.0$, **b** $x = 0.1$, **c** $x = 0.2$, and **d** $x = 0.3$

Table 2 Particle sizes by SEM (D_{SEM}) and TEM (D_{TEM}) of $La_{1-x}Sm_xFeO_3$ ($x = 0.0$, 0.1, 0.2, and 0.3) nanoparticles with the weight (%) of elements in samples

$La_{1-x}Sm_xFeO_3$	D_{SEM} (nm)	D_{TEM} (nm)	Element, weight (%)			
			O-K	C-K	Fe-K	La-K
$x = 0.0$	57.87 ± 4.88	56.48 ± 3.22	29.12	10.91	33.34	34.63
$x = 0.1$	42.56 ± 2.84	42.86 ± 3.19	31.96	12.62	14.98	16.42
$x = 0.2$	29.76 ± 5.89	35.25 ± 2.43	33.34	28.07	28.61	28.01
$x = 0.3$	19.84 ± 6.27	23.21 ± 4.40	34.63	27.35	23.07	20.94

plane consistent with those of the XRD results. The EDX results in Fig. 3 clearly show that all doped samples contain La, Fe, Sm, and O atoms with high Sm peak intensity in samples of high Sm content. The weight (%) of La, Fe, O, and C atoms, as summarized in Table 2, are quantitatively calculated from the EDX spectra and it is found that La atom decreases in samples of high Sm content, resulting from the substitution of Sm atom on the La site. According to the limitation of our instrument, the weight (%) of Sm can be qualitatively determined, which is found to increase in a proper amount correspond with the doping level of Sm in $La_{1-x}Sm_xFeO_3$ ($x = 0.0$, 0.1, 0.2, and 0.3) samples. It can be seen in Table 2 that the weight (%) of Fe atom is insignificantly vary, while those of O and C atoms increase in samples with high amount of Sm atom. The appeared Cu peaks come from the copper grid. Homogeneous distribution of $La_{1-x}Sm_xFeO_3$ ($x = 0.0$, 0.1, 0.2, and 0.3) nanoparticles can be observed by SEM images in Fig. 4. The calculated average particle sizes (D_{SEM}) of samples using Image J program are summarized in Table 2. Similarly, D_{SEM} are found to decrease from 57.87 ± 4.88 to 19.84 ± 6.27 nm, which are comparable to D_{TEM}.

FTIR spectra of $La_{1-x}Sm_xFeO_3$ ($x = 0.0$, 0.1, 0.2, and 0.3) nanoparticles are shown in Fig. 5. All peaks at ~1492.85 cm^{-1} are assigned to C=O stretching mode, corresponding to the vibration of a carbonization group. In addition, the absorption peak at ~1635.61 cm^{-1} is attributed to C–O–C stretching mode, corresponding to the surface-adsorbed oxygen species and organic substances, whereas that at ~3449.94 cm^{-1} is assigned for the stretching and bending modes of the O–H bond [34, 38]. From these results, it is suggested that heat treatment can promote the carbonization of organic substances as well as the crystallization of nanoparticles. Moreover, the strong absorption peaks at ~563.42 cm^{-1} and a lower one are attributed to

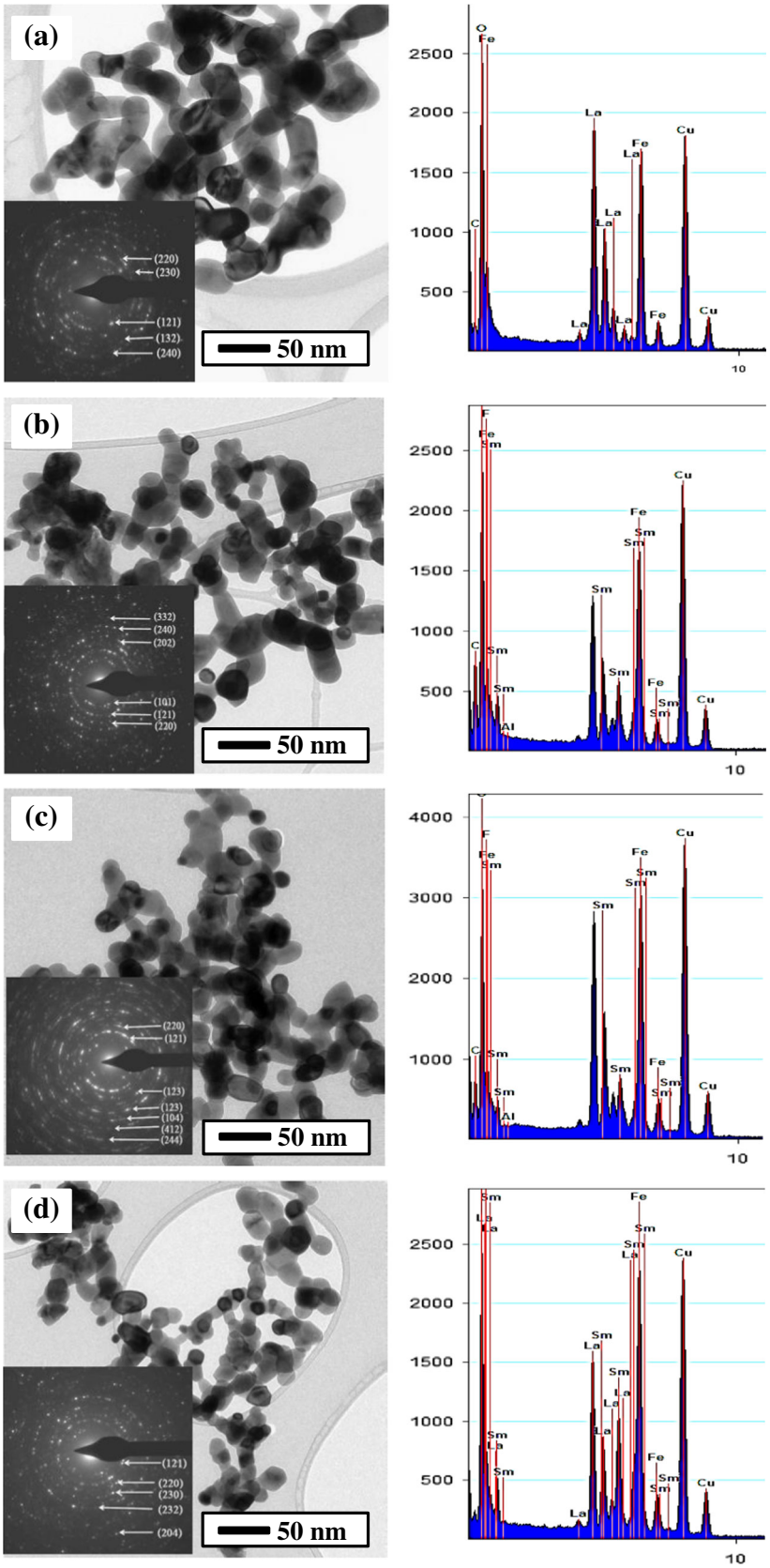

Fig. 3 TEM bright field images with inset of the corresponding SAED patterns of $La_{1-x}Sm_xFeO_3$ nanoparticles. **a** $x = 0.0$, **b** $x = 0.1$, **c** $x = 0.2$, and **d** $x = 0.3$

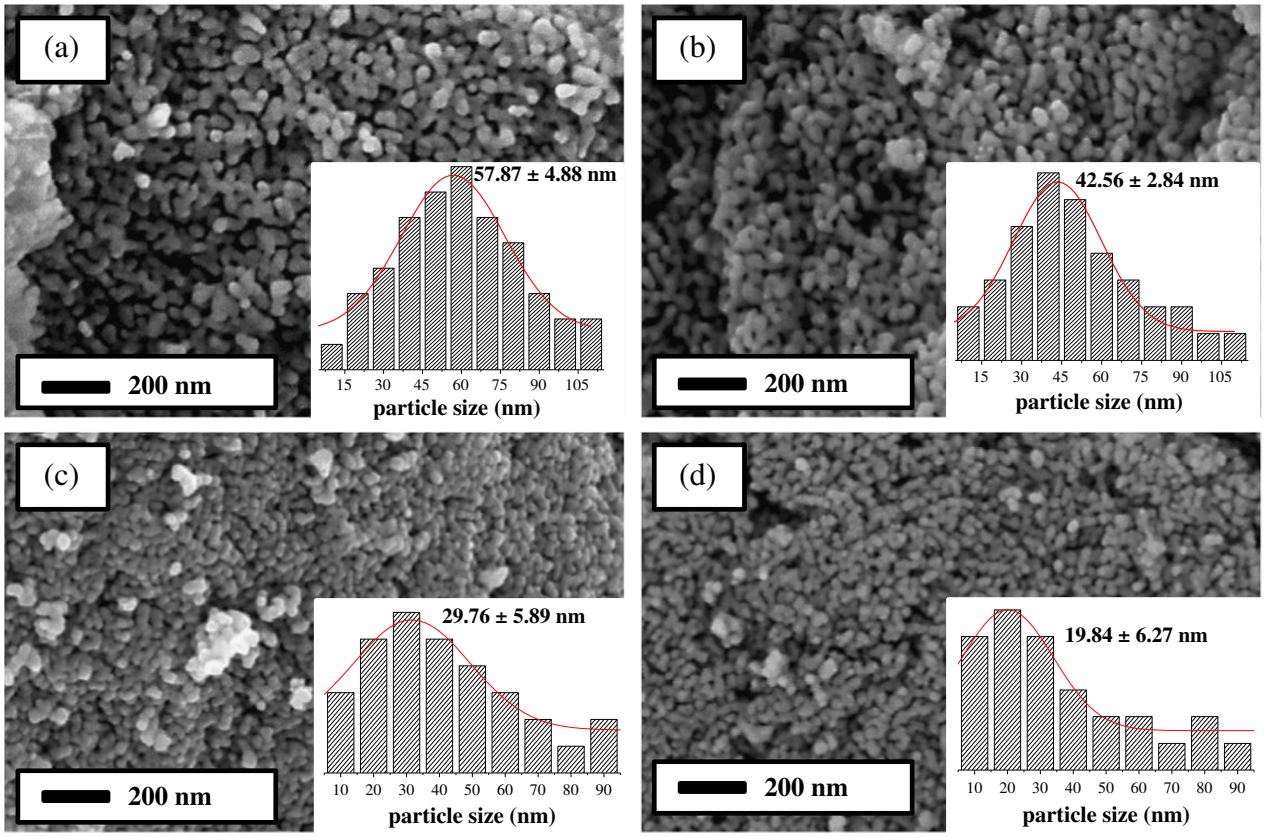

Fig. 4 SEM images of $La_{1-x}Sm_xFeO_3$ nanoparticles. **a** $x = 0.0$, **b** $x = 0.1$, **c** $x = 0.2$, and **d** $x = 0.3$

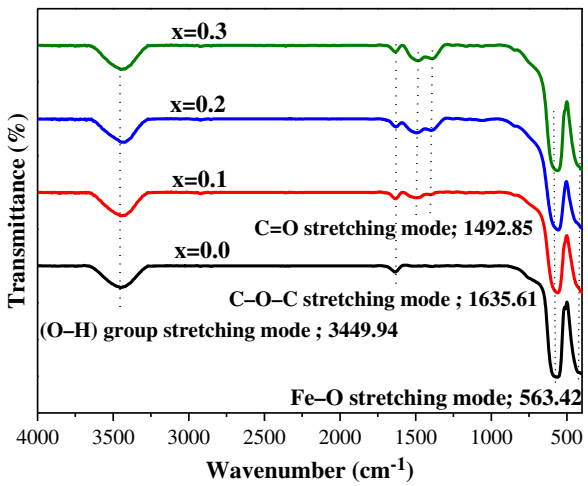

Fig. 5 FTIR spectra of $La_{1-x}Sm_xFeO_3$ ($x = 0.0$, 0.1, 0.2, and 0.3) nanoparticles

Fe–O stretching vibration, being characteristics of the octahedral FeO_6 groups in the perovskite compounds.

The XPS spectra of $La_{0.7}Sm_{0.3}FeO_3$ sample measured for a chemical analysis of surface and the oxidation state of various ions are shown in Fig. 6. The binding energies of La $3d_{5/2}$ at 833.726 and 837.943 eV, and La $3d_{3/2}$ at 850.431 and 854.843 eV corresponds to La^{3+} ion, whereas those of Fe $2p_{3/2}$ at 710.027 eV and Fe $2p_{1/2}$ at 724.051 eV corresponds to Fe^{3+} ion [21, 35, 38, 39]. The O (*1s*) main peak at 529.212 eV corresponds to oxygen ion in the perovskite. The O (*1s*) peaks at 530.304 and 531.471 eV are probably due to an absorbed oxygen (O^{2-}) of water molecule or hydroxyl group (OH^-), since the O (*1s*) binding energy of O^{2-} or OH^- ion is generally 2.1–2.5 eV higher than that of lattice oxygen [21, 35, 38]. However, these samples are easily hygroscopic when they are exposed to air, thus the peak at 531.471 eV is considered probably due to a water molecule associated with the surface.

The normalized Fe K-edge XANES spectra of $La_{1-x}Sm_xFeO_3$ ($x = 0.0$ and 0.3) nanoparticles and those of Fe-standard metals with different oxidation states are shown in Fig. 7. All XANES spectra at Fe K-edge were measured in a transmission mode at room temperature. It is clearly seen in Fig. 7 that the edge positions of FeO (Fe^{2+}), Fe_3O_4 (Fe^{2+}, Fe^{3+}), and Fe_2O_3 (Fe^{3+}) standards appear at approximately 7120, 7122, and 7124 eV, respectively. Clearly, the shift of the edge positions appear at approximately 7126 and 7127 eV for samples of $x = 0.0$ and

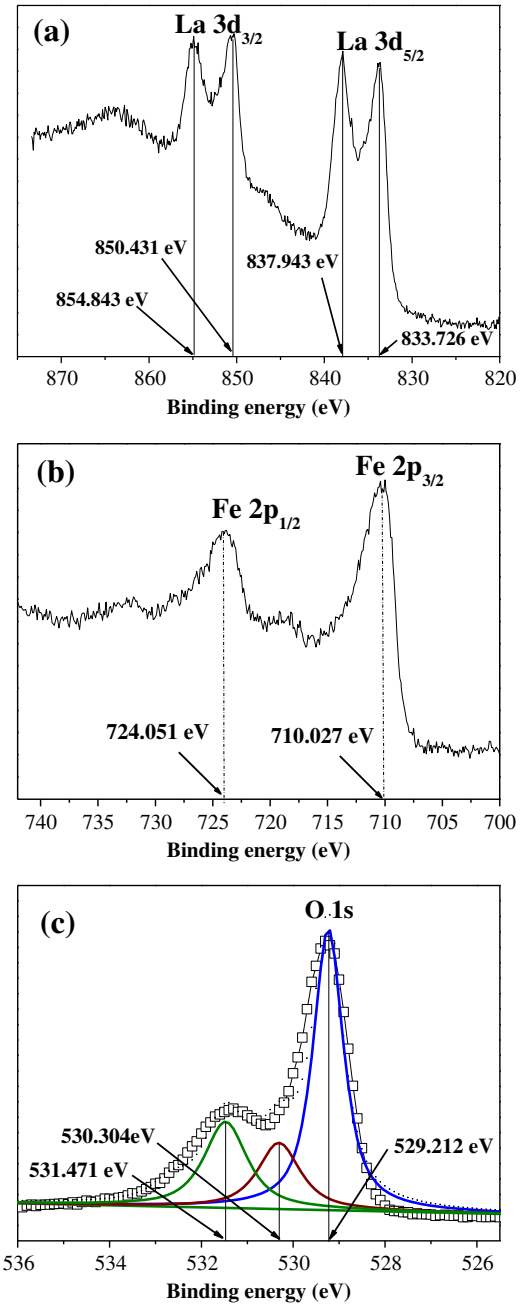

Fig. 6 XPS spectra of **a** La(*3d*), **b** Fe(*2p*), and **c** O(*1s*) of $La_{0.7}Sm_{0.3}FeO_3$ nanoparticles

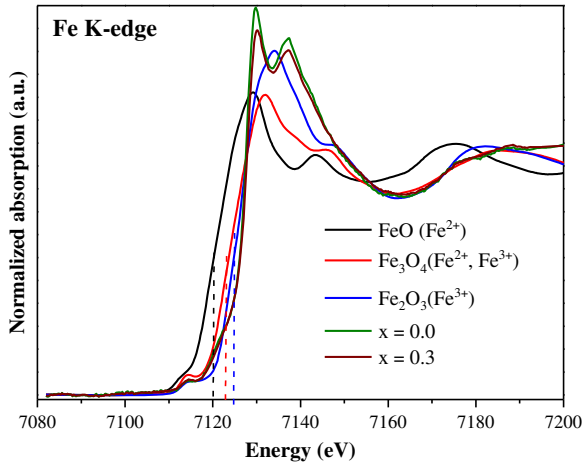

Fig. 7 Fe K-edge XANES spectra of the standards Fe foil, FeO (Fe^{2+}), Fe_3O_4 (Fe^{2+}, Fe^{3+}) and Fe_2O_3 (Fe^{3+}) with those of the $La_{1-x}Sm_xFeO_3$ ($x = 0.0$ and 0.3) nanoparticles

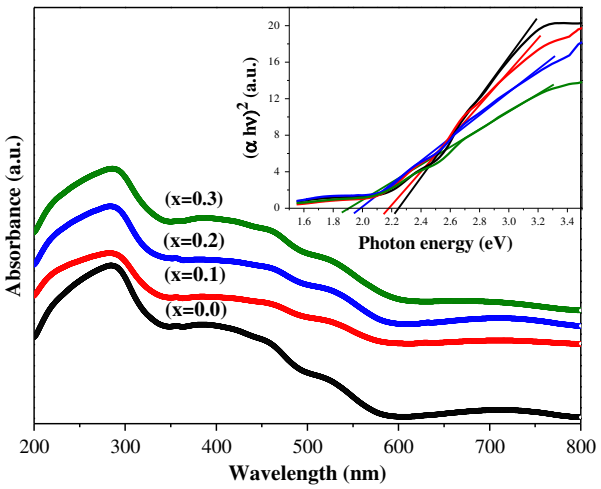

Fig. 8 UV–vis spectra of $La_{1-x}Sm_xFeO_3$ ($x = 0.0$, 0.1, 0.2 and 0.3) nanoparticles with the inset of $(\alpha h\nu)^2$ plots as a function of photon energy

0.3, which close to that of the Fe^{3+} standard, indicating the valence state of +3 for Fe ion in these samples [2, 21, 26].

The UV–vis spectra of $La_{1-x}Sm_xFeO_3$ ($x = 0.0$, 0.1, 0.2, and 0.3) nanoparticles are shown in Fig. 8 with an obviously broad-absorption peak centered at approximately 285 nm. From the plot of $(\alpha h\nu)^2$ vs. $h\nu$, shown by an inset in Fig. 8, the optical band gaps (*Eg*) of these samples can be determined by extrapolating the slope to the zero value of $(\alpha h\nu)^2$ and the *Eg* values are found to be 2.218, 2.198, 1.959, and 1.880 eV for samples of $x = 0.0$, 0.1, 0.2, and 0.3, respectively. These values are monotonically decreased with the increase of Sm content as summarized in Table 3. It is obvious that Sm doping can significantly decrease the particle sizes and band gaps of $LaFeO_3$. This confirms that

Table 3 Optical band gap (E_g), magnetization (*M*), remanent magnetization (M_r), and coercive field (H_c) of $La_{1-x}Sm_xFeO_3$ ($x = 0.0$, 0.1, 0.2, and 0.3) nanoparticles

$La_{1-x}Sm_xFeO_3$	E_g (eV)	*M* at 30 kOe (emu/g)	M_r (emu/g)	H_c (Oe)
$x = 0.0$	2.218	0.382	–	–
$x = 0.1$	2.198	0.580	0.003	95.07
$x = 0.2$	1.959	0.776	0.160	4387.79
$x = 0.3$	1.880	1.135	0.467	13,062.79

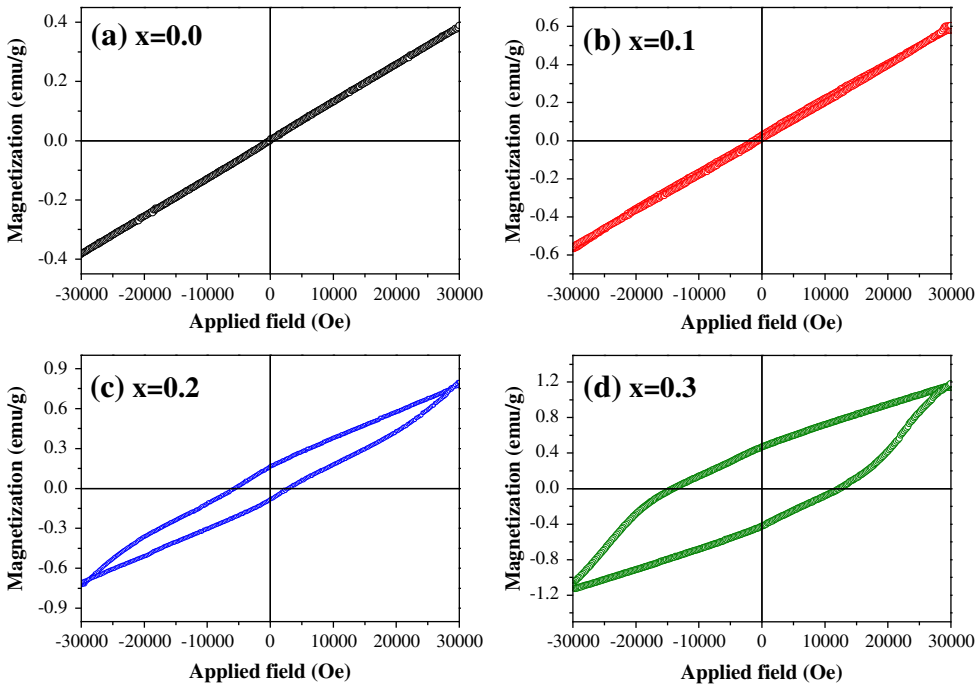

Fig. 9 Magnetization at room temperature of $La_{1-x}Sm_xFeO_3$ nanoparticles as a function of external field. **a** $x = 0.0$, **b** $x = 0.1$, **c** $x = 0.2$, and **d** $x = 0.3$

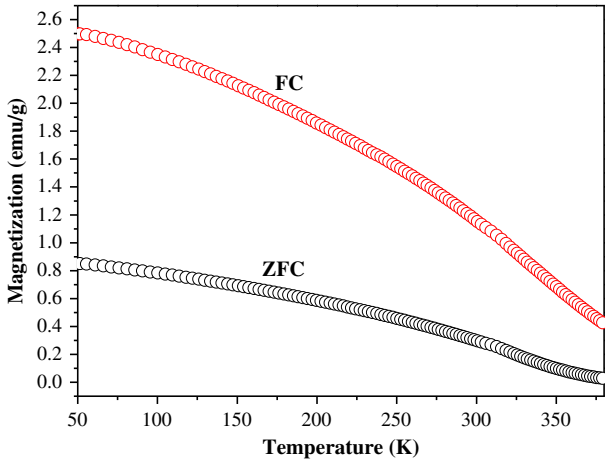

Fig. 10 Temperature dependence of magnetization of $La_{0.7}Sm_{0.3}FeO_3$ nanoparticles in zero field-cooled (ZFC) and field-cooled (FC) modes at a constant external field H of 10 kOe

Sm^{3+} ion can affect the optical transition in $La_{1-x}Sm_xFeO_3$ ($x = 0.0$, 0.1, 0.2 and 0.3) nanoparticles.

The room temperature magnetizations of $La_{1-x}Sm_xFeO_3$ ($x = 0.0$, 0.1, 0.2, and 0.3) samples measured by VSM are shown in Fig. 9. The *M-H* curve of undoped sample is very narrow, indicating the antiferromagnetic behavior of sample, whereas those of the Sm-doped $LaFeO_3$ samples with $x = 0.1$, 0.2, and 0.3 show larger loops of magnetizations belong to those of ferromagnetic behavior with increasing magnetizations (M), H_c, and remanent magnetizations (M_r) as summarized in Table 3. However, the coercive field are significantly increased to 13,062.79 Oe for $La_{0.7}Sm_{0.3}FeO_3$ sample, which is approximately 137 times higher than the value of 95.07 Oe for a sample of $x = 0.05$. Moreover, this value of 13,062.79 Oe is approximately 2.46 and 2.78 times higher than those obtained values of 5308.4 and 4702.326 Oe in our previous works of $La_{0.7}Al_{0.3}FeO_3$ [20] and $La_{0.7}Ga_{0.3}FeO_3$ [21], respectively. The enhancements of M, H_c, and M_r are suggested to originate from the structure distortion and size reduction due to the decrease of lattice parameters as a result of Sm doping. These results confirm the important of size effect on ferromagnetic behavior in perovskite oxides [20–26, 40, 41]. The temperature dependence of magnetization behavior of $La_{0.7}Sm_{0.3}FeO_3$ sample under ZFC and FC modes measured in an external magnetic field of 10 kOe from 50 to 380 K are shown in Fig. 10. In Fig. 10, the magnetizations of this sample in both FC and ZFC measurements gradually decrease with the increase of temperature due to the thermal fluctuations causing the randomization of polarization direction of magnetic moment [8, 20]. It can be seen in Fig. 10 that the zero value of both magnetizations cannot be observed in the temperature range of measurement, implying that the Curie temperature (T_c) is above 400 K [2, 20, 26].

4 Conclusions

$La_{1-x}Sm_xFeO_3$ ($x = 0.0$, 0.1, 0.2, and 0.3) nanoparticles can be successfully prepared by sol–gel method. XRD results indicate the orthorhombic phase of nanoparticles with the decrease of lattice parameters, crystallite sizes, and cell volumes due to the substitution of small ionic radius of Sm^{3+} ion on the La^{3+} site in the orthorhombic perovskite

structure, resulting in the distortion of the crystal structure and particle sizes reduction. The calculated crystallite sizes of samples by Scherrer equation are consistent with those obtained by Williamson-Hall equation. Williamson-Hall plots show the increase of microstrain in samples of high Sm content as a result of the decrease in lattice parameters. SEM and TEM images show nanoparticles of almost spherical shape in high Sm-doped samples with the decrease of average particle sizes ranging from 57.87 ± 4.88 to 19.84 ± 6.27 nm. The determined optical band gaps decrease from 2.218 to 1.880 eV with increasing Sm content. XPS and XANES results indicate the oxidation state 3+ for La and Fe ions in the perovskite structure. Undoped sample exhibits antiferromagnetic behavior, whereas doped samples exhibit ferromagnetic behavior as confirmed by VSM results. The coercive field can be enhanced to a very high value of 13,062.79 Oe for a sample of $x = 0.3$ with the estimated Curie temperature (T_c) above 400 K.

Acknowledgments This work was financially supported by the Integrated Nanotechnology Research Center (INRC), Department of Physics, Faculty of Science, Khon Kaen University, Thailand. Financial assistance also comes from the Higher Education Research Promotion and National Research University Project of Thailand, Office of the Higher Education Commission and the Nanotechnology Center (NANOTEC), NSTDA, Ministry of Science and Technology, Thailand through its program of Center of Excellence Network. Thanks are due to Rajamangala University of Technology Rattanakosin Wang Klai Kangwon Campus, Thailand (Grant A21/2559) for co-providing financial support.

Compliance with ethical standards

Conflict of interest The authors declare that they have no competing interests.

References

1. Dixon CAL, Kavanagh CM, Knight KS, Kockelmann W, Morrison FD, Lightfoot P (2015) Thermal evolution of the crystal structure of the orthorhombic perovskite $LaFeO_3$. J Solid State Chem 230:337
2. Ciambelli P, Cimino S, De Rossi S, Lis L, Minelli G, Porta P, Russo G (2001) $AFeO_3$ (A = La, Nd, Sm) and $LaFe_{1-x}Mg_xO_3$ perovskites as methane combustion and CO oxidation catalysts: structural, redox and catalytic properties. Appl Catal B 29:239
3. Phokha S, Pinitsoontorn S, Rujirawat S, Maensiri S (2015) Polymer pyrolysis synthesis and magnetic properties of $LaFeO_3$ nanoparticles. Physica B 476:55
4. Hao Hung M, Madhava Rao MV, Shyang Tsai D (2007) Microstructures and electrical properties of calcium substituted $LaFeO_3$ as SOFC cathode. Mater Chem Phys 101:297
5. Wang Y, Yang X, Lu L, Wang X (2006) Experimental study on preparation of $LaMO_3$ (M = Fe, Co, Ni) nanocrystals and their catalytic activity. Thermochim Acta 443:225
6. Khetre SM, Chopade AU, Khilare CJ, Kulal SR, Jadhav HV, Jagadale PN, Bangale SV, Bamane SR (2014) Ethanol gas sensing properties of nano-porous LaFeO3 thick films. J of Shivaji Uni (Sci & Tech) 41(2):250–5347
7. Minh DL, Mai Hoa VN, Ngoc Dinh N, Thi Thuy N (2013) Electric and thermoelectric properties of $LaFeO_3$ compounds doped by Ti, Co and Cu ions. VNU J Mathematics Physics 29(3):42
8. Paul Blessington Selvadurai A, Pazhanivelu V, Jagadeeshwaran C, Murugaraj R, Panneer Muthuselvam I, Chou FC (2015) Influence of Cr substitution on structural, magnetic and electrical conductivity spectra of $LaFeO_3$. J Alloys Compd 646:924
9. Phokha S, Hunpratup S, Pinitsoontorn S, Putasaeng B, Rujirawat S, Maensiri S (2015) Structure, magnetic, and dielectric properties of Ti-doped $LaFeO_3$ ceramics synthesized by polymer pyrolysis method. Mater Res B 67:118
10. Thirumalairajan S, Girija K, Mastelar VR, Ponpandian N (2015) Investigation on magnetic and electric properties of morphologically different perovskite LaFeO3 nanostructures. J Mater Sci: Mater Electron. 26:8652–8662
11. Acharya S, Mondal J, Ghosh S, Roy SK, Chakrabarti PK (2010) Multiferroic behavior of lanthanum orthoferrite ($LaFeO_3$). Mater Lett 64:415
12. Xu X, Guoqiangn T, Huijun R, Ao X (2013) Structural, electric and multiferroic properties of Sm-doped $BiFeO_3$ thin films prepared by the sol–gel process. Ceram Inter 39:6223
13. Mazumder R, Ghosh S, Mondal P, Bhattacharya D, Dasgupta S, Das N, Sen A, Tyagi AK, Sivakumar M, Takami T, Ikuta H (2006) Particle size dependence of magnetization and phase transition near TN in multiferroic $BiFeO_3$. J Appl Phys 100:1
14. Todd MR, Gary LC, James MA (1993) Combined magnetic-dipole and electric-quadrupole hyperfine interactions in rare-earth orthoferrite ceramics. Phys Rev B 48:224
15. Treves D (1965) Studies on Orthoferrites at the Weizmann Institute of Science. J Appl Phys 36:1033
16. Kodama RH, Berkowitz AE (1999) Atomic-scale magnetic modeling of oxide nanoparticles. Phys Rev B 59:6321
17. Lee YC, Parkhomov AB, Krishnan KM (2010) Size-driven magnetic transitions in monodisperse MnO nanocrystals. J Appl Phys 107: 09E124-1-3.
18. Fujii T, Matsusue I, Nakatsuka D, Nakanishi M, Takada J (2011) Synthesis and anomalous magnetic properties of $LaFeO_3$ nanoparticles by hot soap method. Mater Chem Phys 129:805
19. Köferstein R, Jäger L, Ebbinghaus SG (2013) Magnetic and optical investigations on $LaFeO_3$ powders with different particle sizes and corresponding ceramics. Solid State Ionics 249:1
20. Janbutrach Y, Hunpratub S, Swatsitang E (2014) Ferromagnetism and optical properties of $La_{1-x}Al_xFeO_3$ nanopowders. Nanoscale Res Lett 9:498
21. Hunpratub S, Karaphun A, Phokha S, Swatsitang E (2016) Optical and magnetic properties of $La_{1-x}Ga_xFeO_3$ nanoparticles synthesized by polymerization complex method. Appl Surf Sci 380:52
22. Barbero B, Gamboa JA, Cadus LE (2006) Synthesis and characterisation of $La_{1-x}Ca_xFeO_3$ perovskite-type oxide catalysts for total oxidation of volatile organic compounds. Appl Catal B 65:21
23. Shikha P, Kang TS, Randhawa BS (2015) Effect of different synthetic routes on the structural, morphological and magnetic properties of Ce doped $LaFeO_3$ nanoparticles. J Alloys Compd 625:336
24. Prasad BV, Rao BV, Narsaiah K, Rao GN, Chen JW, Babu DS (2015) Preparation and characterization of perovskite Cu doped $LaFeO_3$ semiconductor ceramics. IOP Conf Series: Mater Sci Eng 73:012129
25. Chandrasekhar KD, Mallesh S, Murthy JK, Das AK, Venimadhav A (2014) Role of defects and oxygen vacancies on dielectric and

magnetic properties of Pb^{2+} ion doped $LaFeO_3$ polycrystalline ceramics. Physica B 448:304
26. Phokha S, Hunpratup S, Pinitsoontorn S, Maensiri S (2015) Structure, magnetic, and dielectric properties of Ti-doped $LaFeO_3$ ceramics synthesized by polymer pyrolysis method. Mater Res Bull 67:118
27. Lüning J, Nolting F, Scholl A, Ohldag H, Seo JW, Fompeyrine J, Locquet J-P, Stöhr J (2003) Determination of the antiferromagnetic spin axis in epitaxial LaFeO3 films by x-ray magnetic linear dichroism spectroscopy. Phys Rev B 67:214433
28. Li S, Wang X (2015) Synthesis of different morphologies lanthanum ferrite ($LaFeO_3$) fibers via electrospinning. Optik 126:408
29. Xiao H, Xue C, Song P, Li J, Wang Q (2015) Preparation of porous $LaFeO_3$ microspheres and their gas-sensing properties. Appl Surf Sci 337:65
30. Tang P, Tong Y, Chen H, Cao F, Pan (2013) Microwave-assisted synthesis of nanoparticulate perovskite LaFeO3 as a high active visible-light photocatalyst. Appl Phys 13:340
31. Sivakumar M, Gedanken A, Zhong W, Jiang YH, Du YW, Brukental I, Bhattacharya D, Yeshurunc Y, Nowikd I (2004) Sonochemical synthesis of nanocrystalline $LaFeO_3$. J Mater Chem 14:764
32. Velichkova MM, Lazarova T, Tumbalev V, Ivanov G, Kovacheva D, Stefanov P, Naydenov A (2013) Complete oxidation of hydrocarbons on $YFeO_3$ and $LaFeO_3$ catalysts. Chem Eng J 231:236
33. Kansara SB, Dhruv D, Joshi Z, Pandy DD, Rayaprol S, Solanki PS, Kuberkar DG, Shah NA (2015) Structure and microstructure dependent transport and magneticproperties of sol–gel grown nanostructured $La_{0.6}Nd_{0.1}Sr_{0.3}MnO_3$ manganites: role of oxygen. Appl Surf Sci 356:1272
34. Liua T, Xu Y (2011) Synthesis of nanocrystalline $LaFeO_3$ powders via glucose sol–gel route. Mater Chem Phys 129:1047
35. Yang Z, Huang Y, Dong B, Li HL (2006) Controlled synthesis of highly ordered $LaFeO_3$ nanowires using a citrate-based sol–gel route. Mater Res B 41:274
36. Cullity BD, Stock SR (2001) Elements of X-ray Diffraction. 3rd edn, Prentice-Hall, Upper Saddle River, NJ
37. Majeed Khan MA, Kumar S, Ahamed M (2015) Structural, electrical and optical properties of nanocrystalline silicon thin films deposited by pulsed laser ablation. Mat Sci Semicon Proc 30:169
38. Cho YG, Choi KH, Kim YR, Jung JS, Lee SH (2009) Characterization and catalytic properties of surface La-rich $LaFeO_3$ perovskite. Bull Korean Chem Soc 30:6
39. Lee WY, Yun HJ, Yoon JW (2014) Characterization and magnetic properties of $LaFeO_3$ nanofibers synthesized by electrospinning. J Alloys Compd 583:320
40. Jaiswal A, Das R, Maity T, Vivekan K, Abraham PM, Adyanthaya S, Poddar P (2010) Temperature-dependent raman and dielectric spectroscopy of $BiFeO_3$ nanoparticles: signatures of spin-phonon and magnetoelectric coupling. J Phys Chem C 114:2108
41. Schuele WJ, Deetscreek VD (1962) Appearance of a weak ferromagnetism in fine particles of antiferromagnetic materials. J Appl Phys 33:1136